Electrochemically exfoliated thin Bi2Se3 films and van der Waals heterostructures Bi2Se3/graphene

To cite this article before publication: Irina Antonova *et al* 2019 *Nanotechnology* in press https://doi.org/10.1088/1361-6528/ab5cd5

IOP Publishing Journal Title
Journal **XX** (XXXX) XXXXXX https://doi.org/XXXX/XXXX

Electrochemically exfoliated thin Bi_2Se_3 films and van der Waals heterostructures Bi_2Se_3/graphene

I V Antonova,[1,2,3] N A Nebogatikova,[1,2] K A Kokh,[2,4] D A Kustov,[2] R A Soots,[1] V A Golyashov,[1] O E Tereshchenko[1,2]

[1] Rzhanov Institute of Semiconductor Physics SB RAS, Novosibirsk, 630090, Russia
[2] Novosibirsk State University, Novosibirsk, 630090, Russia
[3] Novosibirsk State Technical University, Novosibirsk, 630073, Russia
[4] Sobolev Institute of Geology and Mineralogy SB RAS, Novosibirsk, 630090, Russia

E-mail: : antonova@isp nsc ru, E-mail: nadonebo@gmail com

Received xxxxxx
Accepted for publication xxxxxx
Published xxxxxx

Abstract

Thin Bi_2Se_3 flakes with few nanometer thicknesses and sized up to 350 μm were created by using the electrochemical splitting from high-quality Bi_2Se_3 bulk monocrystals. The dependence of film resistance on the Bi_2Se_3 flake thickness demonstrates that, at room temperature, the bulk conductivity becomes negligible in comparison with the surface conductivity for films with thicknesses lower than 80 nm. Unexpectedly, all these films demonstrated the p-type conductivity. The doping effect with sulfur or sulfur-related radicals during electrochemical exfoliation is suggested for the p-type conductivity of the exfoliated Bi_2Se_3 films. The formation of 2-8 nm films was predominantly found. Van der Waals (vdW) heterostructures Bi_2Se_3/Graphene/SiO_2/Si were created and their properties were compared with that of Bi_2Se_3 on the SiO_2/Si substrate. The increase of the conductivity and carrier mobility in Bi_2Se_3 flakes of 3-5 times was found for vdW heterostructures with graphene. Thin Bi_2Se_3 films are potentially interesting for applications for spintronics, nano- and optoelectronics.

Keywords **b**ismuth selenide, electrochemical exfoliation, van der Waals heterostructures, electrical properties, carrier mobility

1 Introduction

The tremendous interest in the electronic properties of topological insulators (TIs), such as Bi_2Se_3, Bi_2Te_3, Sb_2Te_3, and some other chalcogenide materials stems from the fact that they have robust topological surface states (TSS) [1-3]. TIs are characterized by intrinsic insulating bulk states and metallic surface states due to strong spin-orbit coupling. The Dirac-like surface states in topological insulators are protected by the time-reversal symmetry, which naturally forbids backscattering events during the carrier transport process and, therefore, suggests promising applications in dissipationless spintronic devices [4], while the TSS is predicted to have peculiar properties of great interest for future electronic devices in spintronics and quantum computation [5,6]. The current researches usually focus on Bi_2Se_3, which has a relatively large band gap in its bulk (~0.3 eV). The conducting bulk is usually more prevalent in Bi_2Se_3 crystals and films due to the existence of vacancies and impurities. Therefore, it is difficult to manipulate independently with the conduction from the TSS. Films of ultra-small thickness are demonstrated as an effective way

for TIs to control and suppress the bulk contribution to transport [7-9].

The multiple conductive channels are found to coexist for thicker films: bulk, impurity band, and surface states. It is shown that in Bi_2Te_3 for thicknesses 10-30 nm, for the TSS channel, the carrier mobility can reach ~5600 - 6000 cm^2/Vs at the temperature of 2 K, almost one order of magnitude larger than the bulk mobility (860 cm^2/Vs) [7]. For the thickness of 6 nm, the Bi_2Se_3 film mobility of bulk electrons exhibits a power-law $\mu \propto T^{-2}$ at high temperatures, which suggests the mechanism of phonon scattering and a room temperature value of μ = 700 cm^2/Vs [8]. At low temperatures (T < 20 K), the mobilities of both impurity band and surface states reach constant values of ~380 and ~5000 cm^2/Vs, respectively.

The sheet resistance as a function of temperature typically shows different dependences. If the resistance exponentially increases as the temperature decreases, this is most likely associated with the carrier activation through the bulk bandgap. The activation energy is generally increased with a decrease in the film thickness [10,11]. If the resistance is reduced as the temperature decreases, resembling the metallic behavior widely observed in TIs it corresponds to alleviated phonon scatterings. In case that the resistance approaches constant values, this temperature regime is believed to be dominated by the surface conduction [11].

As a rule, thin (< 10 nm) films of bismuth chalcogenides were created by means of different types of exfoliation (mechanical exfoliation [12], electrochemical exfoliation [13]) or different types of growth, or deposition [see, e g , 14] or synthesis [15]. These approaches allow one to obtain flakes sized ~ 20-50 μm. Moreover, thinner flakes have, as a rule, smaller sizes. Small Bi_2Se_3 nanoparticles have attracted huge attention in biological and medical applications as a material for the *in vivo* protection against the ionizing radiation based on their superior antioxidant activities and electrocatalytic properties [16]. But, generally, large-scaled thin TIs films are required for studies and applications.

In this study, we report on the approach which allows one to create high quality Bi_2Se_3 thin films with relatively large sizes (up to 350 μm) by using the electrochemical splitting from Bi_2Se_3 bulk monocrystals. The films have, as a rule, the thicknesses of 2-8 nm, the resistivity of 8 – 80 kOhm/sq, the p-type conductivity and carrier mobilities of 20-60 cm^2/Vs. The vdW heterostructures created by the transfer of thin Bi_2Se_3 films on graphene/SiO_2/Si lead to an increase in the carrier mobility (up to 150-180 cm^2/Vs) and a decrease in the film resistivity by a factor of 4-6 times down to 2-4 kOhm/sq.

2 Methods

2 1 Bi_2Se_3 thin film preparation

The electrochemical exfoliation of thin films from a high-quality monocrystalline bulk Bi_2Se_3 occurred due to the formation of gas bubbles between the layers during the electrolysis and creation of the flakes on the solution surface, after which they can be transferred to the desired substrate Bi_2Se_3 acted as a cathode, a Pt wire as an anode and $(NH_4)_2S_2O_8$ or Na_2SO_4 with the concentration of 1% served as electrolyte with similar results. During exfoliation, there occurred water hydrolyzes, the intercalation of H_2SO_4 into the bulk Bi_2Se_3, formation of gaseous H_2 and NH_3 gas bubbles at the cathode, which provided an exfoliation of Bi_2Se_3 flakes [17,18]. By varying the voltage, time, type and concentration of the electrolyte, it was found that it is possible to obtain various sizes and thicknesses of the resulting films. Voltages of the order of 2-5 V and the exfoliation time lower than 5 minutes turned out to be optimal. For the high exfoliation time in the $(NH_4)_2S_2O_8$ solution, Bi_2Se_3 flakes are destroyed and small nanoparticles (Se nanoparticle, as it is demonstrated by the Raman spectra below) are the main result of exfoliation.

Another successful option was the exfoliation in an electrolyte based on the 0.1 M aqueous solution of H_2SO_4 Relatively large (up to 500 μm) flakes with thicknesses 10–30 nm were obtained. The other alternative option was the delamination in the electrolyte based on HCl or an aqueous solution of NaOH, but the exfoliation of Bi_2Se_3 was not observed. Most likely, in these cases, there is no successful intercalated agent (like H_2SO_4). All types of created flakes with their parameters are shown in Table 1. After the splitting, the flakes were transferred onto oxidized silicon substrates; the oxide thickness was ~ 300 nm.

2 2 Experimental techniques

The Raman spectra were recorded on a Horiba Jobin Yvon LabRAM HR800 spectrometer with a 1024-pixel LN/CCD detector and an Nd:Gd 532 nm laser under ambient conditions. A Solver PRO NT-MDT scanning microscope was employed for taking AFM images from the surface of the examined films and for evaluating the sample thicknesses. The measurements were carried out in contact and semi-contact modes. The current-voltage characteristics were measured with a Keithley picoamperemeter (model 6485) on film samples provided with two contacts prepared from the silver alloy. The silver alloy was applied onto the film surface as a contact. SEM images were obtained using a JEOL JSM-7800F scanning electron microscope in which the energy of primary electrons was equal to 2 keV.

3 Results and Discussion

The most typical thickness of the flakes obtained in 1% $(NH_4)_2S_2O_8$ or Na_2SO_4 electrolytes was 4 nm. The characteristic dimensions were up to 200–300 μm. The films with larger thicknesses are destroyed during the exfoliation process (see Fig. 1 cd) due to the poor mechanical properties of this material (for the bulk Bi_2Se_3 material Young modulus E = 70.3 GPa Poisson ratio σ = 0.281 [17]). We suppose that there is a kind of mechanical instability for Bi_2Se_3 films with thicknesses of more than 8 nm due to destruction fragility on the cohesion boundaries of domains.

Within a large number of flakes (~ 30 samples) with the predominant thickness of 4 nm, only two surviving flakes with the thicknesses of 12 and 23 nm were obtained. In addition, a large number of nanoparticles sized ~20-30 nm was formed. These films were transferred onto the SiO_2/Si substrate for further characterization. The flakes were also used for the creation of vdW heterostructures on graphene/SiO_2/Si substrates. The exfoliation sketch and AFM images of Bi_2Se_3 films transferred on SiO_2/Si substrates are given in Fig. 1 and Fig. 2a. It was revealed with the use of Raman spectroscopy that nanoparticles consist of Se (see Fig. 2b). To reduce their density on the surface of Bi_2Se_3 flakes, we used treatment in the 4 % water solution of NH_3, but it was not possible to remove all Se nanoparticles.

The chemical stability of $B_{i2}Se_3$ (0001) was found to be quite good for high-quality single crystals [18-20]. The stability of our flakes in the air is limited by the time of few months; during 4-6 months, AFM images and electrical properties of Bi_2Se_3 flakes were unchanged. Generally, a strong degradation of thin films during the air storage can be expected dependently on the technique used for flake creation [20]. The surface degradation and formation of holes are really found in the flakes. We suggest that degradation is connected with the formation of Se vacancy due to the electrochemical exfoliation process in the films and film oxidation.

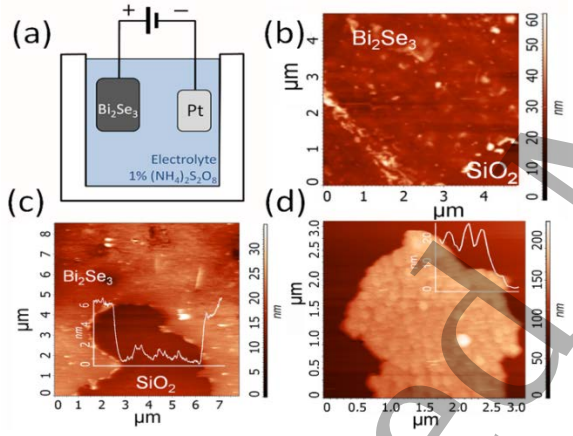

Fig. 1 (a) Scheme of electrochemical splitting setup. After the exfoliation, the films were transferred onto the SiO_2/Si substrates. (b,c) AFM images of Bi_2Se_3 films with thickness 4 and 6 nm, respectively. Typical film thickness was in the range of 2-8 nm. The Bi_2Se_3 film in (b) has a high density of Se nanoparticles on the surface and under the film. (d) AFM images of Bi_2Se_3 films with a thickness of ~20 nm.

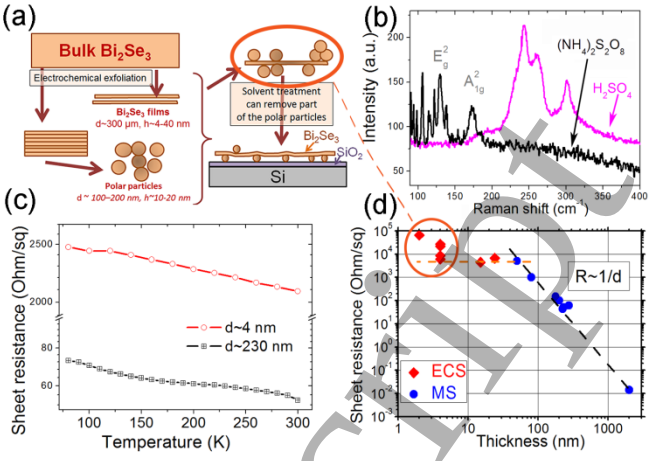

Fig. 2 (a) Sketch of the exfoliation process Bulk Bi_2Se_3 can be split off by the electrochemical exfoliation into thin films. (b) Raman spectra of the Bi_2Se_3 films obtained using different electrolytes ($(NH_4)_2S_2O_8$ and H_2SO_4). (c) Temperature dependence of Bi_2Se_3 films sheet resistance with thickness ~4 with Se nanoparticles on the surface and ~230 nm. (d) Sheet resistance ($R_{\square}$, Ohm/sq) for Bi_2Se_3 films depending on their thickness. The given data were obtained for different approaches to the film production: ECS is for the flakes created by electrochemical exfoliation, MS is for the flakes created by the mechanical exfoliation from the same bulk crystal.

According to the Raman spectroscopy, the exfoliated flakes have different properties for $(NH_4)_2S_2O_8$ and H_2SO_4 electrolytes (Fig. 2b). Two characteristic peaks were observed at 130 cm^{-1} and 173 cm^{-1}, which are typical of Bi_2Se_3 lattice vibrations and correspond to the in-plane mode (E_{g2}^2) and the out-of-plane mode (A_{1g}^2), respectively [22-24]. The ratio of these peak intensities indicates a small thickness of the obtained films. The additional lines observed in the case of the $(NH_4)_2S_2O_8$ electrolyte in the range of 80 – 170 cm^{-1} can be connected with the intercalation of the different ions [24]. When the aqueous solution of H_2SO_4 was utilized as an electrolyte, another set of peaks was observed in the film spectra in positions ~ 240, ~ 260, ~ 300 cm^{-1}. The peak intensity ratio could vary for different points and films. The peaks near 240 and 260 cm^{-1} are related to the formation of a selenium layer [25]. The BiO_x modes are located in Raman spectra at 250 cm^{-1} and 328 cm^{-1} [26]. These peaks are generally related to the dangling bonds that appeared on the Bi_2Se_3 film surface as a result of the Se vacancies which easily react with oxygen atoms of the environment and form BiOx [27,28].

Table 1. Results of the exfoliation process in the different electrolytes

Electrolyte	Exfoliation time, min	Flake size, □m	Thickness, nm	Resistivity kOhm/sq	Material type
0.1 mM $(NH_4)_2S_2O_8$ or Na_2SO_4	< 5	30 – 350	4±2	8-80	Bi_2Se_3 flakes
0.1 mM $(NH_4)_2S_2O_8$	> 2	0.02-0.10	10-20	> 10^4	Se nanoparticles
0.1 M H_2SO_4	5 - 10	200 -1000	10 - 30	> 10^4	Bi_2Se_3 flakes
0.1 M HCl	5 - 30	-	-	-	No exfoliation
0.1 M NaOH	5 - 30	-	-	-	No exfoliation

So, the flakes are oxidized with a Se-rich layer on the surface. Similar results were obtained by the chemical analysis of films by SEM. It is the reason why the films obtained with the H_2SO_4 electrolyte were non-conductive. These peaks are not found in the films obtained with the use of $(NH_4)_2S_2O_8$ electrolytes. Note, that the observed peaks are not related to the formation of the high conductive Bi_2O_2Se material [29].

The sheet resistance ($R_{\square}$, Ohm/sq) for Bi_2Se_3 films versus their thickness is given in Fig. 2d. The given data were obtained for two different approaches used for the film creation, i e electrochemical and mechanical exfoliations. The resistivity for both film types demonstrated the expected dependence when a reduction in thickness d leads to an increase in resistance $R_{\square} = R_{bulk} + R_S$, where bulk resistance $R_{bulk} \sim 1/d$ and R_S is the surface channel resistance. The saturation of this curve with a decrease in d corresponds to the value of surface channel resistance R_S in the range of 8 – 80 kOhm/sq. The R_S value is found to be very sensitive to the Se nanoparticle density. To decrease the Se nanoparticles number, we use the NH_3-treatment. It leads to a decrease in R_S from 80 to 8 kOhm/sq. Value of R_S = 8-9 kOhm/sq was well reproduced for the case of low Se nanoparticle density and this R_S for the electrochemically exfoliated flakes is practically equal to values of R_S obtained for the mechanically exfoliated flakes (thickness ~20 – 80 nm). It means that the surface channel is survived after electrochemical exfoliation process Increase in resistivity for films with Se particles is connected with charges carried by these nanoparticles. This observation means that the surface has to be cleaned from Se nanoparticles for the surface channel domination in the conductivity.

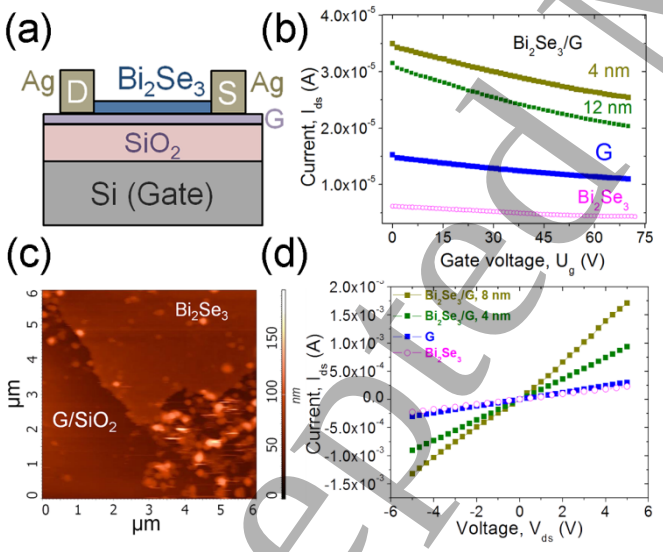

Fig. 3 (a) Schematic image of transistor characteristics with the back silicon gate. (b,d) $I_{ds}(U_g)$ and $I_{ds}(V_{ds})$ measurements for Bi_2Se_3, graphene, Bi_2Se_3/G films (thicknesses 4 nm and 8 nm), the CVD-grown graphene film (d~0 35 nm) and Bi_2Se_3/G heterostructures (d~4 and 8 nm). The drain-source voltage for (b) was 100 mV. (c) 4 nm- Bi_2Se_3 film transferred onto graphene/SiO_2/Si. There are Se nanoparticles near the bottom Bi_2Se_3 edge.

One of the transistor characteristics measured with the use of the Si substrate as a gate (see, Fig. 3a) is presented in Fig. 3b. The typical values of carrier mobility in thin Bi_2Se_3 films with thicknesses 2-8 nm are found to be equal to 25 – 55 cm^2/Vs.

The temperature dependences of Bi_2Se_3 film sheet resistances with thicknesses ~4 and ~230 nm are given in Fig. 2c. The semiconductor behavior of both films looks different in comparison with the bulk metallic temperature dependence of the bulk Bi_2Se_3 material [30,31]. Moreover, the semiconductor behavior of the sheet resistances is typically observed for the thin Bi_2Se_3 film [for instant, 3,32]. According to [33] this temperature dependence of resistance is described by the two-dimensional electron-electron interaction.

Table 2 Electrical parameters of the Bi_2Se_3 films created in $(NH_4)_2S_2O_8$ electrolytes in comparison with vdW Bi_2Se_3/G/SiO_2/Si heterostructures. R is the Bi_2Se_3sheet resistivity, μ is the hole mobility.

Structures	d, Bi_2Se_3, nm	R, kOhm/sq	μ, cm^2/Vs
Bi_2Se_3/SiO_2/Si	2-8	8 - 80	25 - 60
G/SiO_2/Si	-	6 7	48
Bi_2Se_3/G/SiO_2/Si	4	4 4	180
Bi_2Se_3/G/SiO_2/Si	8	2 1	166

Now consider the electrical properties of vdW Bi_2Se_3/G/SiO_2/Si heterostructures. Two heterostructures were created by using the Bi_2Se_3 films with thicknesses 4 and 8 nm. The current-voltage characteristics for these heterostructures (transistor-like structures, see Fig.3a) $I_{ds}(V_{ds})$ and $I_{ds}(U_g)$ are shown in Fig. 3b,d, and the estimated resistance and charge carrier mobility are given in Table 2. Carrier mobility was calculated from the linear part of $I_{ds}(V_g)$ characteristics and with use of the expression $\mu = \frac{\Delta I_{DS}}{\Delta V_G}\frac{1}{C_{SiO_2} V_{DS}\frac{W}{L}}$, , where C_{SiO2} is the specific capacitance of the oxide layer on the surface of the silicon substrate (oxide thickness 300 nm, ε ~ 3.9), *W* and *L* are the width and length of the tested structure.

The Bi_2Se_3/G/SiO_2/Si heterostructures demonstrate the p-type conductivity, decrease in the sheet resistivity, and enhanced carrier mobility (see Fig. 3 and Table 2). The mobility for the Bi_2Se_3/G/SiO_2/Si heterostructure (~160-180 cm^2/Vs) is larger than that for the Bi_2Se_3 films on SiO_2 substrate (~20-60 cm^2/Vs). The low carrier mobility in the graphene connected with the procedure of Bi_2Se_3 flake transfer. The graphene not covered with Bi_2Se_3 flakes-due to chemical treatments without annealing has the carrier mobility of about ~50 cm^2/Vs. Before the film transfer, the carrier mobility in graphene on the SiO_2/Si substrate was ~1100 cm^2/Vs. That, the utilization of CVD-graphene as a substrate for Bi_2Se_3 vdW heterostructures leads to the increase in the film conductivity and enhanced carriers mobility of 3-5 times:

Different proximity effects are observed in vdW TI/G heterostructures. In the theoretical study of Song [34], it was demonstrated that enhancing the spin−orbit interaction in graphene, via proximity effects with topological insulators, could create a novel 2D system that combines nontrivial spin textures with high electron mobility. The spin textures of surface states in a topological insulator can be directly transferred to graphene by means of the proximity effect, which is very important for realizing a two-dimensional topological insulator based on graphene [35]. A strain caused by the graphene layer reduces the bandgap of surface states, and the band bending resulting from the charge transfer at the Bi_2Se_3−graphene interface induces localization of surface states to each top and bottom layer to suppress the overlapping of the two surface states [36]. Cao [37] shows explicitly how strong hybridization between Dirac fermions in graphene and the surface states of topological insulators can reduce the Fermi velocity of Dirac fermions. We have demonstrated positive changes in the parameters of vdW Bi_2Se_3/G/SiO_2/Si heterostructure in comparison with that of Bi_2Se_3/SiO_2/Si due to proximity effect.

The proximity effect was observed for Bi_2Se_3 flakes with a thickness of 4 - 8 nm. In the case of thin films, this material becomes flexible [38]. Moreover, we have used CVD graphene and its wrinkles were no obstacle to the proximity effect observed in Bi_2Se_3.

The Bi_2Se_3 thin films deposited on quartz/glass and mica substrates were found to be n-type due to the native defects, such as Se_{Bi} antisites and/or Se vacancies, acting as active n-type dopants with charge carrier concentrations in the range of ~10^{18} -·10^{19} cm^{-3} [39,5]. The atomic layer deposition of bismuth sulfide (Bi_2S_3) is known to lead to p-type conductivity [40]. The thin Bi_2Se_3 films doped with Ca ($Bi_{2-\delta}Ca_\delta Se_3$ $\delta \geq 0.0025$) also demonstrate their p-type conductivity of ~10^{19} cm^{-3} [41]. In the case of thin films created by means of the electrochemical exfoliation from Bi_2Se_3 bulk monocrystals in 1% $(NH_4)_2S_2O_8$ or Na_2SO_4 electrolytes, the doping effect with sulfur or sulfur-related radicals during the exfoliation process is suggested for the observed p-type conductivity.

Generally, chemical exfoliation has the same graphene-like shortcomings, such as the small size of nanosheets with a variation of thickness and single-layer separation difficulties [42]. Nevertheless, the lateral size of exfoliated Bi_2Se_3 nanosheets obtained by this method reaches ~300 μm, which is one order larger than that of chemically or mechanically exfoliated Bi_2Se_3 nanosheets. The high quality of the used monocrystals allows one to create atomically smooth films of a large area.

Conclusions

Finally, it is shown that, for Bi_2Se_3 films with thicknesses of ≤ 80 nm, the contribution of the bulk conductivity can be neglected. It was found that Bi_2Se_3 films with thicknesses of 2-8 nm have the p-type conductivity with a sheet resistance of ~ 8-80 kOhm/sq, and carrier mobilities of ~ 20-60 cm^2/Vs at room temperature can be obtained with the use of electrochemical exfoliation. Thin conductive layers (2-8 nm) with lateral dimensions up to 350 μm and a wide range of characteristics were obtained by the electrochemical exfoliation of Bi_2Se_3 single crystals. The doping effect with sulfur or sulfur-related radicals during the electrochemical exfoliation is suggested for the p-type conductivity of thin Bi_2Se_3 films. For vdW Bi_2Se_3/G/SiO_2/Si heterostructures, the increase in the carrier mobility (up to 160-180 cm^2/Vs) and enhanced conductivity of Bi_2Se_3 layers were demonstrated. So, we have demonstrated the positive changes in the parameters of vdW Bi_2Se_3/G/SiO_2/Si heterostructure created from electrochemically exfoliated thin films in comparison with those of Bi_2Se_3/SiO_2/Si. These proximity effects observed in vdW Bi_2Se_3/G/SiO_2/Si heterostructures could open interesting opportunities for new device functionalities and applications.

Acknowledgments

This work was supported by the RFBR grant No. 18-29-12094 and the state assignment of IGM SB RAS. The study has also been supported by the Russian Science Foundation (Grant No. 17-12-01047) in part of the single crystal growth.

References

[1]. Chiatti O, Riha C, Lawrenz D, Busch M, Dusari S, Sánchez-Barriga J, Mogilatenko A, Yashina L V, Valencia S, Ünal A A, Rader O, and Fischer S F 2016 *Sci Rep* **6** 27483
[2]. Hasan M Z and Kane C L 2010 *Rev Mod Phys* **82** 3045
[3]. Majhi K, Pal K, Lohani H, Banerjee A, Mishra P, Yadav A K, Ganesan R, Sekhar B R, Waghmare U V, and Kumar P S A 2017 *Appl Phys Lett* **110** 162102
[4]. Wang Y, Xiu F, Cheng L, He L, Lang M, Tang J, Kou X, Yu X, Jiang X, Chen Z, Zou J and Wang K L 2012 *Nano Lett* **12** 1170
[5]. Vedeneev S I 2017 *Physics-Uspekhi* **60** 385
[6]. Huang Y Q, Song Y X, Wang S M, Buyanova I A and Chen W M (2017) *Nature Com* **8** 15401
[7]. Mo D L, Wang W B, and Cai Q 2016 *Nanoscale Research Lett* **11** 354
[8]. He L, Xiu F, Yu X, Teague M, Jiang W, Fan Y, Kou X, Lang M, Wang Y, Huang G, Yeh N-C and Wang K L 2012 *Nano Lett* **12** 1486
[9]. Bansal N, Kim Y S, Brahlek M, Edrey E and Oh S 2012 *Phys Rev Let* **109** 116804
[10]. Zhang Y, He K, Chang C-Z, Song C-L, Wang L-L, Chen X, Jia J-F, Fang Z, Dai X, Shan W-Y, Shen S-Q, Niu Q, Qi X-L, Zhang S-C, Ma X-C, and Xue Q-K 2010 *Nat Phys* **6** 584
[11]. He L, Xiu F, Wang Y, Fedorov A V, Huang G, Kou X, Lang M, Beyermann W P, Zou J and Wang K L 2011 *J Appl Phys* **109** 103702
[12]. Shahil K M F, Hossain M Z, Goyal V and Balandin A A 2012 *J Appl Phys* **111** 054305
[13]. Teweldebrhan D, Goyal V and Balandin A A 2010 *Nano Lett* **10** 1209
[14]. Wang W J, Gao K H and Li Z Q 2016 *Sci Rep* **6** 25291
[15]. Min Y, Moon G D, Kim B S, Lim B, Kim J-S, Kang C Y and Jeong U 2012 *J Am Chem Soc* **134** 2872

[16]. Zhang X-D, Jing Y, Song S, Yang J, Wang J-Y, Xue X, Min Y, Park G, Shen X, Sun Y-M and Jeong U 2017 *Nanomedicine Nanotech Bio Medic* **13** 1597
[17]. Gao X, Zhou M, Cheng Y, and Ji G 2016 *Philosophical Magazine* **96** 208
[18]. Golyashov V A, Kokh K A, Makarenko S V, Romanyuk K N, Prosvirin I P, Kalinkin A V, Tereshchenko O E, Kozhukhov A S, Sheglov D V, Eremeev S V, Borisova S D, and Chulkov E V , 2012 J Appl Phys **112** 113702
[19]. Tereshchenko O E, Kokh K A, Atuchin V V, Romanyuk K N, Makarenko S V, Golyashov V A, Kozhukhov A S, Prosvirin I P and Shklyaev A A 2011 *JETP Letters* **94** 465
[20]. Komonov A I, Prinz V Y, Seleznev V A, Kokh K A and Shlegel V N 2017 *Appl Surf Sci* **410** 1
[21]. Lang M, He L, Xiu F, Yu X, Tang J, Wang Y, Kou X, Jiang W, Fedorov A V and Wang K L, 2012 *ACS Nano* **6**, 295
[22]. Zhang J, Peng Z P, Soni A, Zhao Y, Xiong Y, Peng B, Wang J, Dresselhaus M S and Xiong Q 2011 *Nano Lett* **11** 2407
[23]. Chis V, Sklyadneva I Yu, Kokh K A, Volodin V A, Tereshchenko O E and Chulkov E V 2012 *Phys Rev B* **86**, 174304
[24]. Ambros A and Pumera I M, 2018 *Chem Soc Rev* **47**, 7213
[25]. Poborchii V V 1998 *Appl Phys Lett* **72** 1167
[26]. Zhang J, Yang C, Liu M, Jiang S, Zhang C, Sun Z, Liu F, Xu Y and Man B 2015 *Front Nanosci Nanotech* **1** 19
[27]. Liu F Y, Liu M, Liu A H, Yang C, Chen C S, Zhang C, Bi D and Man B 2015 *J Mater Sci* **26** 3881
[28]. Kong D S, Cha J J, Lai K J, Peng H L, Analytis J G, Meister S, Chen Y, Zhang H J, Fisher I R, Shen Z X and Cui Y 2011 *ACS Nano* **5** 4698
[29]. Sultana R, Gurjar G, Patnaik S and Awana V P S 2019 *J Supercond Nov Magn* **32** 769
[30]. Mao Q, Geng X, Yang J, Zhang J, Zhu S, Yu Q, Wang Y, Li H, Li R and Hao H 2018 *J Crystal Growth* **498** 244
[31]. Wu J, Yuan H, Meng M, Chen C, Sun Y, Chen Z, Dang W, Tan C, Liu Y, Yin J, Zhou Y, Huang S, Xu H Q, Cui Y, Hwang H Y, Liu Z, Chen Y, Yan B and Peng H 2017 *Natur Technol* **12** 530
[32]. Xu Y, Miotkowski I, Liu C, Tian J, Nam H, Alidoust N, Hu J, Shih C-K, Hasan M Z, and Chen Y P. 2014 *Nat Phys* **10** 956.
[33]. Shikin A M, Klimovskikh I I, Eremeev S V, Rybkina A A, Rusinova M V, Rybkin A G, Zhizhin E V, Sanchez-Barriga J, Varykhalov A, Rusinov I P, Chulkov E V, Kokh K A, Golyashov V A, Kamyshlov V, Tereshchenko O E, 2014 *Phys Rev B* **89** 125416.
[34]. Song K, Soriano D, Cummings A W, Robles R, Ordejón P and Roche S 2018 *Nano Lett* **18** 2033
[35]. Zhang L, Lin B-C, Wu Y-F, Wu H-C, Huang T-W, Chang C-R, Ke X, Kurttepeli M, Tendeloo G V, Xu J, Yu D, and Liao Z M. 2017 *ACS Nano* **11** 6277
[36]. Chae J, Kang S-H, Park S H, Park H, Jeong K, Kim T H, Hong S-B, Kim K S, Kwon Y-K, Kim J W and Cho M -H 2019 *ACS Nano* **13** 3931
[37]. Cao W, Zhang R -X, Tang P, Yang G, Sofo J, Duan W, Liu C -X 2016 *2D Mater* **3** 034006
[38]. Peng H, Dang W, Cao J, Chen Y, Wu D, Zheng W, Li H, Shen Z-X, Liu Z 2012 *Nat. Chem.***4** 281**.**
[39]. Xue L, Zhou P, Zhang C X, He C Y, Hao G L, Sun L Z, Zhong J X 2013 *AIP Advances* **3** 052105
[40]. Mahuli N, Saha D, Sarkar S K 2017 *J Phys Chem C* **121** 8136
[41]. Hsieh D, Xia Y, Qian D, Wray L, Dil J H, Meier F, Osterwalder J, Patthey L, Checkelsky J G , Ong N P, Fedorov A V, Lin H , Bansil A, Grauer D , Hor Y S, Cava R J , Hasan M Z 2009 *Nature* **460** 1101
[42]. Yang Y, Hou H, Zou G, Shi W, Shuai H, Li J Ji X 2019 *Nanoscale* **11** 16